Accepted Manuscript

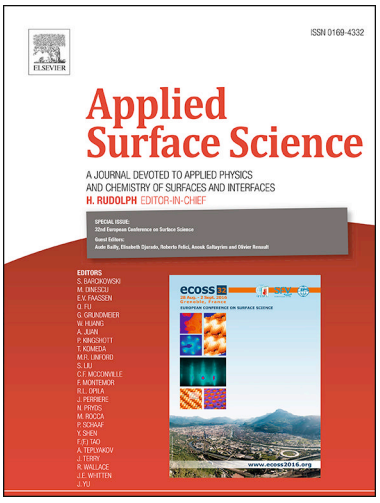

Full Length Article

Nanocrystalline $CeO_{2-\delta}$ coated β-MnO_2 nanorods with enhanced oxygen transfer property

Xiubing Huang, Guixia Zhao, Yueqi Chang, Ge Wang, John T.S. Irvine

PII: S0169-4332(17)33791-1
DOI: https://doi.org/10.1016/j.apsusc.2017.12.197
Reference: APSUSC 38067

To appear in: *Applied Surface Science*

Received Date: 14 October 2017
Revised Date: 8 December 2017
Accepted Date: 21 December 2017

Please cite this article as: X. Huang, G. Zhao, Y. Chang, G. Wang, J.T.S. Irvine, Nanocrystalline $CeO_{2-\delta}$ coated β-MnO_2 nanorods with enhanced oxygen transfer property, *Applied Surface Science* (2017), doi: https://doi.org/10.1016/j.apsusc.2017.12.197

Nanocrystalline $CeO_{2-\delta}$ coated β-MnO_2 nanorods with enhanced oxygen transfer property

Xiubing Huang,[a,b] Guixia Zhao,[b] Yueqi Chang,[a] Ge Wang[a*] and John T.S. Irvine[b]*

[a] Beijing Key Laboratory of Function Materials for Molecule & Structure Construction, School of Materials Science and Engineering, University of Science and Technology Beijing, Beijing, 100083, China.

[b] School of Chemistry, University of St Andrews, St Andrews, Fife, KY16 9ST, UK.

*Corresponding authors: Prof. Ge Wang (gewang@mater.ustb.edu.cn) and Prof. John T. S. Irvine (jtsi@st-andrews.ac.uk)

Abstract: In this research, β-MnO_2 nanorods were synthesized by a hydrothermal method, followed by a facile precipitation method to obtain nanocrystalline $CeO_{2-\delta}$ coated β-MnO_2 nanorods. The as-prepared samples were characterized by XRD, HRTEM, FESEM, XPS and in-situ high-temperature XRD. The HRTEM results show that well dispersed $CeO_{2-\delta}$ nanocrystals sized about 5 nm were coated on the surface of β-MnO_2 nanorods. The oxygen storage and transfer property of as-synthesized materials were evaluated using TGA under various atmospheres (air, pure N_2, and 5%H_2/95%Ar). The TGA results indicate that $CeO_{2-\delta}$ modification could favour the reduction of Mn^{4+} to Mn^{3+} and/or Mn^{2+} at lower temperature as compared with pure β-MnO_2 nanorods and the physically mixed $CeO_{2-\delta}$-β-MnO_2 under low oxygen partial pressure conditions (i.e., pure N_2, 5%H_2/95%Ar). Specifically, $CeO_{2-\delta}$@β-MnO_2 sample can exhibit 7.5 wt% weight loss between 100 and 400 ^oC under flowing N_2 and 11.4 wt% weight loss between 100 and 350 ^oC under flowing 5%H_2/95%Ar. During the reduction process under pure N_2 or 5%H_2/95%Ar condition, the oxygen ions in β-MnO_2 nanorods are expected to be released to the surroundings in the form of O_2 or H_2O with the coated $CeO_{2-\delta}$ nanocrystals acting as mediator as inferred from the synergistic effect between the well-interacted $CeO_{2-\delta}$ nanocrystals and β-MnO_2 nanorods.

Keywords: $CeO_{2-\delta}$; β-MnO_2; oxygen transfer; synergetic effect

1. Introduction

Oxygen storage materials (OSMs) that can store/release oxygen at elevated temperature or changeable oxygen partial pressure have potential applications in numerous oxygen-related energy and environmental fields, especially in catalysis.[1, 2] For example, OSMs based on ceria can be used as three-way catalysts for the conversion of automobile exhaust emissions (e.g., NO_x, CO, and hydrocarbons) into harmless gases and H_2O.[3] Since fuel (such as methane, CO, soot) oxidation into harmless CO_2 and H_2O is of great importance to environmental protection and energy utilization, it is necessary to develop efficient and effective OSMs for the fuel oxidation reaction at relatively low temperatures. It is also crucial to comprehensively understand the mechanism of oxygen storage, transfer and release in OSMs.

In the past several years, OSMs based on transition metal species (e.g., Cu, Fe, Mn, Co) have attracted considerable attention due to their relatively low cost but high catalytic activity, as well as their changeable valences.[4-6] As an important transition metal element with variable oxidation states, manganese oxides (MnO_2, Mn_2O_3, Mn_3O_4, or MnO), especially MnO_2, have been widely studied as catalysts and catalyst supports for oxidation reactions because of their redox capabilities, high oxygen storage capacity in the crystalline lattice, abundant amount, relatively low price and environmental friendliness.[7-12] However, the catalytic activity of pure MnO_2 is still not high enough, which may result from the poor oxygen transfer in pure MnO_2 at low temperature.[13] Various strategies have been adopted to improve the catalytic activity and oxygen transfer of MnO_2, such as reducing their particle size to nanoscale and doping MnO_2 with other metal elements.[14, 15] Recently, it has been indicated that modifying the surface of MnO_2 with noble metals or other metal oxides is an effective strategy to improve their catalytic performance and oxygen transfer property;[16-18] however, the high prices of noble metals limit their wide use. Ceria has been widely utilized as an oxygen carrier owing to the unique redox properties and high oxygen transfer property between CeO_2 and $CeO_{2-\delta}$, but

itself has low oxygen storage capacity (OSC).[19-23] Therefore, it can be imagined that modifying MnO_2 nanomaterials with $CeO_{2-\delta}$ could be an effective strategy to enhance the oxygen transferring by utilizing $CeO_{2-\delta}$ as a possible mediator.[18, 24, 25] Even though the enhanced catalytic performance in CO, C_3H_8, NO, Hg^0 and soot oxidation on Ce-Mn mixed oxides has been contributed to the synergistic effect between Ce and Mn,[24, 26-30] the exact mechanism of synergistic effect between $CeO_{2-\delta}$ and MnO_2, as well as the relationship with surrounding atmospheres is still not clear enough, and needs further exploring.

Herein, we focus on the understanding of oxygen transfer properties between $CeO_{2-\delta}$ and β-MnO_2, as well as their relationship with the surrounding atmospheres. Nanocrystalline $CeO_{2-\delta}$ modified β-MnO_2 nanorods were chosen as the object system, in which β-MnO_2 and $CeO_{2-\delta}$ could mutually benefit by facilitating the oxygen mobility, resulting in enhanced oxygen transfer and release at relatively low temperatures. The understanding of the synergistic effect between $CeO_{2-\delta}$ and β-MnO_2 is also of great importance for the potential applications in catalytic fields.

2. Experimental Section

2.1. Materials synthesis

β-MnO_2 nanorods were synthesized according to the reported procedure.[31] In a typical synthesis, 0.008 mol of $MnSO_4 \cdot H_2O$ (99%, Alfa Aesar) and 0.008 mol of $(NH_4)_2S_2O_8$ (99%, Alfa Aesar) were dissolved into 24 mL of de-ionized water. After 10 min stirring, the mixture was transferred into 40 mL Telfon-lined stainless steel autoclave and kept at 140 ^oC for 12 h. After cooling down to room temperature, the black powder was separated by centrifugation, washed with water 5 times, followed by drying at 80 ^oC for 12 h. The obtained powder was referred to as β-MnO_2-H.

The $CeO_{2-\delta}$ nanocrystals modified β-MnO_2 nanorods were prepared by a room-temperature precipitation method followed by heat-treatment. In a typical process, 0.10 g of obtained β-MnO_2-H was firstly dispersed in the mixture of 70

mL of H_2O and 60 mL of ethanol by ultrasonication for 30 min. After stirring for 2 h, a mixture of 5 mL of H_2O and 0.10 g of $Ce(NO_3)_3 \cdot 6H_2O$ (99%, Sigma-Aldrich) was slowly added into the above solution and the solution was kept stirring for 3 h. Then, a mixture of 5 mL of H_2O and 1 mL of 35 wt% $NH_3 \cdot H_2O$ (Fisher Chemical UK) was added to the above solution. After stirring at room temperature for 24 h, the suspension was separated by centrifugation, washed with H_2O and ethanol for several times. The final product was obtained by drying at 80 ^oC for 1 h, then at 400 ^oC under static air for 4 h and referred to as $CeO_{2-\delta}$@β-MnO_2. For comparison, pure β-MnO_2-H nanorods were treated at 400 ^oC under static air for 4 h to obtain β-MnO_2.

Pure $CeO_{2-\delta}$ nanocrystals were synthesized via a precipitation method.[32] In a typical procedure, 16 mmol of $Ce(NO_3)_3 \cdot 6H_2O$ (99%, Sigma-Aldrich) was dissolved in 5 mL of H_2O in a beaker. Then 35 mL of NaOH (Laboratory reagent grade, Fisher Chemical UK) solution (7 mol/L) was added to the beaker, without stirring or titrating. The suspension was then left at room temperature and pressure for 24 h. The product was washed three times with distilled water and dried at 80 °C for 24 h, followed by calcination at 400 ^oC for 4 h. Then quantitative amounts of calcinated $CeO_{2-\delta}$ nanocrystals and β-MnO_2 nanorods were physically mixed by grinding in a mortar using a pestle. The obtained physical mixture was referred to as $CeO_{2-\delta}$-β-MnO_2, in which the weight ratio of $CeO_{2-\delta}$ to β-MnO_2 is almost the same as that of $CeO_{2-\delta}$@β-MnO_2.

2.2. Characterization

Powder X-ray diffraction (XRD) patterns were recorded at room temperature on a M21X diffractometer (MAC Science Co. Ltd., Japan) using Cu K alpha radiation (λ = 1.541 Å). In situ high-temperature XRD was performed using Mo K alpha radiation (λ = 0.7097 Å) as source under pure N_2 atmosphere from room temperature to 800 ^oC with 100 ^oC as interval. The morphologies of all samples were observed on a ZEISS SUPRA 55 Field Emission Scanning Electron Microscopy (FESEM). High-resolution transmission electron microscope (HRTEM) was performed using a JEOL JEM-2010 electron microscope equipped with energy-dispersive X-ray spectroscopy (EDS) at

200 kV. The samples were prepared by depositing and evaporating a droplet of the sample ethanol solution on a carbon-coated copper grid. Their thermochemical stability and OSC were analyzed by thermogravimetric analysis (TGA) on a NETZSCH STA449C instrument (NETZSCH-Geraetebau GmbH, Selb, Germany) under various gas atmospheres (e.g., air, pure N_2, 5%H_2/95%Ar) with different temperature programs. X-ray photoelectron spectra (XPS) experiments were performed on an ESCALAB 250 spectrometer using Al K alpha radiation. Charging effects were corrected by adjusting in accordance with the binding energy of C1s peak of 284.8 eV. Temperature-programmed reduction with H_2 (H_2-TPR) was performed on an AutoChem II 2920 (Micromeritics, USA). 30 mg of catalyst samples were heated at a rate of 10 K min^{-1} from 30 to 800 ^oC under 10%H_2/90%Ar with a flowing rate of 30 mL/min.

3. Results and Discussion

Fig. 1 presents the X-ray diffraction (XRD) patterns of β-MnO_2, $CeO_{2-\delta}$@β-MnO_2, $CeO_{2-\delta}$-β-MnO_2 and $CeO_{2-\delta}$. All the diffraction peaks in the bottom pattern (Fig. 1a) can be indexed to tetragonal β-MnO_2 with *P42/mnm* space group (JCPDS card No. 24-0735), indicating that the β-MnO_2 structure was maintained even after heat-treatment at 400 ^oC. For $CeO_{2-\delta}$@β-MnO_2 (Fig. 1b), the peaks ascribed to (111), (200), (220), (311), (222), (400), (331) and (420) planes of cubic fluorite-structured $CeO_{2-\delta}$ crystals with *Fm3m* space group (JCPDS card No. 34-0394) were clearly displayed. The obviously broadening peaks which can be ascribed to (200) and (220) of $CeO_{2-\delta}$ demonstrate its nanocrystallite nature, while β-MnO_2 maintained its phase structure. In the physical mixture $CeO_{2-\delta}$-β-MnO_2 (Fig. 1c), there are no obvious peaks of $CeO_{2-\delta}$ due to its small amount as well as the overlay by β-MnO_2 nanorods. Their mean crystalline sizes were determined from XRD line broadening calculation, using the Scherrer Equation: $D = k\lambda/(\beta\cos\theta)$, in which k is Scherrer constant ($k = 0.89$), λ is the X-ray wavelength, β is the line broadening at half maximum intensity (FWHM), and θ is the Bragg angle. The

calculated mean crystal sizes for pure β-MnO_2 (Fig. 1a) and $CeO_{2-\delta}$ in $CeO_{2-\delta}$@β-MnO_2 (Fig. 1b) were ca. 40 and 5 nm, respectively.

Fig. 2 shows the TEM and FESEM images of $CeO_{2-\delta}$, β-MnO_2, $CeO_{2-\delta}$@β-MnO_2 and $CeO_{2-\delta}$-β-MnO_2. The FESEM (Fig. 2a) and TEM (Fig. 2b) images of pure $CeO_{2-\delta}$ exhibited nanorod morphology, similar to reported results.[32] The FESEM (Fig. 2c) and TEM (Fig. 2d) images of pure β-MnO_2 shows that β-MnO_2 nanorods sized from 400 to 2000 nm in length and from 20 to 100 nm in diameter were obtained using the hydrothermal method and heat-treatment at 400 ^oC for 4 h did not change their morphology, similar to reported results.[33] The interplanar spacing of 0.28 nm represented the (001) lattice fringes of β-MnO_2.[34] Both TEM and FESEM results indicate that the surfaces of pure β-MnO_2 nanorods are clean, while the surfaces of β-MnO_2 nanorods in $CeO_{2-\delta}$@β-MnO_2 are homogeneously coated with a large quantity of $CeO_{2-\delta}$ nanocrystals, as shown in the inset of Fig. 2f. The average particle size of $CeO_{2-\delta}$ nanocrystals for $CeO_{2-\delta}$@β-MnO_2 is ca. 5 nm, in agreement with the calculated results from XRD. As shown in the HRTEM (Fig. 2f), the interplanar spacing of 0.31 nm can be indexed to (111) lattice fringes of $CeO_{2-\delta}$ nanocrystals. The FESEM image in Fig. 2g indicates that $CeO_{2-\delta}$ nanocrystals and β-MnO_2 nanorods separately existed in $CeO_{2-\delta}$-β-MnO_2 and there are almost no CeO_2 nanoparticles on the surface of the β-MnO_2. The TEM image for physical mixture $CeO_{2-\delta}$-β-MnO_2 composite in Fig. 2h also shows that $CeO_{2-\delta}$ nanocrystals and β-MnO_2 nanorods are independent, and that only small portion of β-MnO_2 nanorods were adhered with $CeO_{2-\delta}$ nanocrystals. The results indicate that physically mixed $CeO_{2-\delta}$ nanocrystals and β-MnO_2 nanorods do not contact as well as that in $CeO_{2-\delta}$@β-MnO_2.

The XPS spectra of Mn 2p, Ce 3d and O 1s were used to evaluate their oxidation state in $CeO_{2-\delta}$@β-MnO_2, as depicted in Fig. 3. The Mn $2p_{3/2}$ and Mn $2p_{1/2}$ binding energies (Fig. 3a) in $CeO_{2-\delta}$@β-MnO_2 were found to be 642.0 and 653.8 eV, respectively. The two peaks with binding energies of 641.9 eV and 643.6 eV in the deconvolution of Mn $2p_{3/2}$ can be attributed to Mn^{3+} and Mn^{4+},

respectively, which are in good agreement with those reported for MnO_2,[35-37] indicating the oxidation states of Mn species are Mn^{3+} and Mn^{4+} in $CeO_{2-\delta}$@β-MnO_2. Fig. 3b shows the Ce 3d spectra, in which there are six obvious peaks, noted as (V, V", V'") and (U, U", U'"), characteristic of Ce^{4+} final state corresponding to $3d_{5/2}$ and $3d_{3/2}$, respectively.[38] The doublet V at 882.5 eV and U at 901.1 eV were ascribed to the final state Ce^{4+} $4f^2 3d^9$. Doublet V" at 889.2 eV and U" at 907.3 eV were attributed to the final state Ce^{4+} $4f^1 3d^9$, while V'" at 898.4 eV and U'" at 916.7 eV were for the final state of Ce^{4+} $4f^0 3d^9$. There is another doublet V' at 885.2 eV and U' at 903.9 eV which can be ascribed to the XPS spectra of Ce^{3+},[38, 39] indicating the existence of a small amount of Ce^{3+} in $CeO_{2-\delta}$@β-MnO_2. The results indicate that the oxidation state of Ce in $CeO_{2-\delta}$@β-MnO_2 is mainly Ce^{4+} but with some Ce^{3+} due to the sub-stoichiometric state of CeO_{2-x}. The corresponding XPS spectra of O 1s in $CeO_{2-\delta}$@β-MnO_2 is shown in Fig. 3c. By deconvoluting the O 1s spectra, two surface oxygen species (noted as O_α and O_β) are clearly observed. The main band O_α (about 529 eV) represents the characteristic oxygen peak (O^{2-}) of metal oxides[40] while the shoulder O_β with the binding energy around 531 eV may be attributed to the chemisorbed surface species such as O_2^- and O^- with low coordination.[41]

Temperature-programmed reduction profiles of $CeO_{2-\delta}$, β-MnO_2, $CeO_{2-\delta}$@β-MnO_2 and $CeO_{2-\delta}$-β-MnO_2 under flowing 10%H_2/90%N_2 are shown in Fig. 4. Pure $CeO_{2-\delta}$ exhibits two reduction peaks with low intensity at 442 ^oC and 690 ^oC, which correspond to the surface and bulk reduction of CeO_2, respectively.[29] β-MnO_2 exhibited three reduction peaks at 333, 443 and 549 ^oC, which can be ascribed to the reduction of MnO_2 to Mn_2O_3, Mn_3O_4 and MnO. In the cases of $CeO_{2-\delta}$@β-MnO_2, two reduction peaks in the temperature range of 200-300 ^oC and 300-400 ^oC were observed, indicating that the temperature for Mn^{4+} reduction in the $CeO_{2-\delta}$@β-MnO_2 was greatly decreased compared with β-MnO_2 and physically mixed $CeO_{2-\delta}$-β-MnO_2 maybe due to the

enhanced surface exchange oxygen ion mobility between β-MnO_2 and $CeO_{2-\delta}$ species.[29]

TGA analysis is further used to evaluate the oxygen storage and transfer property of as-prepared samples under various atmospheres (e.g., air, pure N_2, 5%H_2/95%Ar), as shown in Fig. 5 and summarized in Table 1. Fig. 5a shows the TGA results of as-prepared samples under air from room temperature to 800 ^oC. The small weight loss from room temperature to 300 ^oC for all these samples under air can be ascribed to the removal of adsorbed water and weakly adsorbed oxygen.[42] The significant weight loss with 6.0-8.3wt% between 550 and 650 ^oC in β-MnO_2, $CeO_{2-\delta}$@β-MnO_2 and $CeO_{2-\delta}$-β-MnO_2 is due to the reduction of MnO_2 to Mn_2O_3 accompanied by the evolution of oxygen, while in $CeO_{2-\delta}$@β-MnO_2 there is another continuous weight loss (2.2 wt%) from 650 to 800 ^oC, which is attributed to the further reduction of partial Mn^{3+} to Mn^{2+}, indicating the positive effect of $CeO_{2-\delta}$ on the oxygen release of β-MnO_2 with elevated temperature under air.

Fig. 5b represents the TGA results of as-prepared samples under pure N_2 from room temperature to 800 ^oC. The TGA curves of $CeO_{2-\delta}$, β-MnO_2 and $CeO_{2-\delta}$-β-MnO_2 under N_2 are similar to those under air, except that the oxygen evolution temperatures under N_2 are just a bit lower than those under air and that there is another continuous weight loss at high temperature for the reduction of partial Mn^{3+} to Mn^{2+}. However, for $CeO_{2-\delta}$@β-MnO_2, low oxygen partial pressure (i.e., pure N_2) could greatly favour the oxygen evolution at low temperature. The $CeO_{2-\delta}$@β-MnO_2 shows obvious weight loss steps under pure N_2. There is a weight loss with about 7.5 wt% occurred at a much lower temperature range (100 and 400 ^oC) than that of pure β-MnO_2 nanorods, which can be ascribed to the removal of oxygen in sub-surface lattices, simultaneously accompanied by the reduction of Mn^{4+} to Mn^{3+} and/or Mn^{2+}. The weight loss at lower temperatures for $CeO_{2-\delta}$@β-MnO_2 could be explained by that $CeO_{2-\delta}$ is easier to release oxygen under inert atmospheres at lower temperature, resulting in quicker oxygen transfer from crystal lattice of β-MnO_2 to $CeO_{2-\delta}$.[42, 43]

The TGA curve of as-prepared samples under flowing 5%H_2/95%Ar is shown in

Fig. 5c. The total weight loss in pure β-MnO_2 (18.8 wt%) is in accord with the theoretical value 18.4 wt% from MnO_2 to MnO. It also clearly shows that β-MnO_2 in $CeO_{2-\delta}$@β-MnO_2 was easier to be reduced to Mn_3O_4 and further to MnO than pure β-MnO_2 and $CeO_{2-\delta}$-β-MnO_2.[44] There is a weight loss of 11.4 wt% in $CeO_{2-\delta}$@β-MnO_2 between 100 and 350 ^oC, further indicating the favour of oxygen mobility from β-MnO_2 nanorods to the highly dispersed $CeO_{2-\delta}$ nanocrystals on the surface of β-MnO_2.[44] However, the poor contact between $CeO_{2-\delta}$ nanocrystals and β-MnO_2 nanorods in physically mixed $CeO_{2-\delta}$-β-MnO_2 lead to a similar weight loss behavior to that of pure β-MnO_2 nanorods. XPS was also used to check the valence of Mn in $CeO_{2-\delta}$@β-MnO_2 after the TGA test from room temperature to 800 ^oC under flowing N_2. The energy separation of 11.8 eV between Mn $2p_{3/2}$ (641.4 eV) and Mn $2p_{1/2}$ (653.2 eV) shown in Fig. 6a is consistent with the corresponding values of Mn_3O_4 in the previous references.[45] The deconvoluted peaks centered at 641.2 eV and 643.1 eV in the spectrum of Mn $2p_{3/2}$ can be attributed to the binding energies of Mn^{2+} and Mn^{3+}, respectively.[46] In the Mn 3s XPS spectrum (Fig. 6b), the two peaks at 83.5 eV and 89.1 eV with the separation of 5.6 eV further confirm the existence of Mn_3O_4.[47]

As indicated by TGA results under pure N_2, $CeO_{2-\delta}$@β-MnO_2 has a three-step weight loss with the increasing of temperature. To further determine the structure changes of $CeO_{2-\delta}$@β-MnO_2 at different temperatures under pure N_2, in-situ high temperature XRD was adopted increasing temperature from room temperature to 800 ^oC with 100 ^oC step, as shown in Fig. 7. The results show that $CeO_{2-\delta}$@β-MnO_2 maintained its structure at 100 ^oC under N_2. However, only a small part of β-MnO_2 was retained at 200 ^oC and a new phase for intermediate MnO_x appeared, indicating β-MnO_2 nanorods in $CeO_{2-\delta}$@β-MnO_2 started to lose lattice oxygen which was located under sub-surfaces of β-MnO_2 at 200 ^oC. Further increasing the temperature to 300 ^oC, only trace β-MnO_2 was observed but the intermediate MnO_x disappeared, and Mn_3O_4 began to form, suggesting β-MnO_2 and intermediate MnO_x may be reduced to Mn_3O_4 at 300 ^oC under pure N_2. Up to 500 ^oC under pure N_2, there

are no obvious changes in the diffraction intensity of $CeO_{2-\delta}$ nanocrystals, revealing the stability of $CeO_{2-\delta}$ nanocrystal size below 500 ^{o}C. With further increasing temperature to 800 ^{o}C, the diffraction peak positions of $CeO_{2-\delta}$ are shifted to lower angles as compared with the standard $CeO_{2-\delta}$, which is due to the loss of some lattice oxygen of $CeO_{2-\delta}$ under flowing N_2. In addition, new peaks attributed to tetragonal Mn_3O_4 (JCPDS card no. 24-0734, space group: I41/amd) were observed from 300 ^{o}C and diffraction peaks ascribed to β-MnO_2 disappeared, indicating Mn_3O_4 was formed under pure N_2 from 300 ^{o}C and their diffraction peaks increased with the increment of temperature. We have also treated pure β-MnO_2 nanorods at 300 ^{o}C under flowing N_2 for 2 h for comparison, and the XRD results in Fig. 8 show that there is no phase change and no peaks ascribed to Mn_3O_4 are observed, which confirmed that oxygen can be transferred from β-MnO_2 at such low temperature under N_2 only with the synergetic effect of $CeO_{2-\delta}$. The in-situ high-temperature XRD results further demonstrate the enhanced oxygen transfer in $CeO_{2-\delta}$@β-MnO_2 system.

Based on the aforementioned results, we propose the arrangement of $CeO_{2-\delta}$@β-MnO_2 and their enhanced oxygen transfer, as shown in Scheme 1. Firstly, β-MnO_2 nanorods from the hydrothermal method were properly homogenously dispersed in the mixture of H_2O and ethanol under continuous stirring. Secondly, after adding $Ce(NO_3)_3{\cdot}6H_2O$, Ce^{3+} cations were adsorbed onto the surface of β-MnO_2 because of the electrostatic interaction between Ce^{3+} cations and negative charged MnO_2 surface from hydrothermal method.[48, 49] Then, OH^- released from $NH_3{\cdot}H_2O$ will in situ react with Ce^{3+} on the nanorod surface to form $Ce(OH)_3$ and/or small CeO_2 nanoparticles in amorphous phase or poor crystal structure.[50] Finally, heat treatment at 400 ^{o}C for 4 h will result in the growth and better crystallinity of non-stoichiometric $CeO_{2-\delta}$ nanocrystals, as demonstrated by XRD, TEM and XPS results. The in-situ growth of non-stoichiometric $CeO_{2-\delta}$ nanocrystals on the surface of β-MnO_2 nanorods would favour their tight contact and the oxygen transfer between $CeO_{2-\delta}$ nanocrystals and β-MnO_2 nanorods. The synergistic

mechanism for enhanced oxygen transfer property in $CeO_{2-\delta}$@β-MnO_2 could be explained by considering the high oxygen removal ability of $CeO_{2-\delta}$ nanocrystals and the closed contact between $CeO_{2-\delta}$ nanocrystals and MnO_2 nanorod surfaces, through which, $CeO_{2-\delta}$ nanocrystals successfully functioned as mediator for the oxygen mobility.[51, 52]

4. Conclusions

In this research, the positive synergistic effect on oxygen transfer in nanocrystalline $CeO_{2-\delta}$ coated β-MnO_2 nanorods was demonstrated. The results show that the good contact between $CeO_{2-\delta}$ nanocrystals and β-MnO_2 nanorods in $CeO_{2-\delta}$@β-MnO_2 is important to the enhanced oxygen mobility. The homogeneously dispersed non-stoichiometric $CeO_{2-\delta}$ nanocrystals on the surface of β-MnO_2 nanorods could favour the oxygen transfer property in β-MnO_2 nanorods under various gases, especially under inert atmospheres (e.g., N_2) and reductive gases (e.g., 5%H_2/95%Ar) to lower temperatures. $CeO_{2-\delta}$@β-MnO_2 sample could exhibit much higher oxygen storage capacity (e.g., 7.5 wt% weight loss between 100 and 400 ^oC under flowing N_2 and 11.4 wt% weight loss between 100 and 350 ^oC under flowing 5%H_2/95%Ar) than that of pure β-MnO_2 nanorods and the physically mixed $CeO_{2-\delta}$-β-MnO_2. It is thought the non-stoichiometic $CeO_{2-\delta}$ acts as inter-mediator for the oxygen mobility from β-MnO_2 to CeO_2 then to surroundings. The in-situ high temperature XRD results have demonstrated the phase change of β-MnO_2 to Mn_3O_4 under pure N_2 at about 300 ^oC. Our research work could provide crucial guidance in the rational design of efficient catalysts with enhanced oxygen mobility at low temperatures.

Acknowledgements

Prof. Ge Wang and Dr. Xiubing Huang acknowledged financial support from the National Key Research and Development Program of China (Grant No. 2016YFB0601100), and Fundamental Research Funds for the Central Universities (FRF-TP-16-028A1). Prof. John T. S. Irvine acknowledged funding from the Engineering and Physical Research Council for research award EP/K036769/1 and

Platform Grant EP/K015540/1, the Royal Society Wolfson Merit Award, WRM 2012/R2.

References

[1] T. Montini, M. Melchionna, M. Monai, P. Fornasiero, Fundamentals and catalytic applications of CeO_2-based materials, Chem. Rev. 116 (2016) 5987-6041.

[2] D. Zhang, X. Du, L. Shi, R. Gao, Shape-controlled synthesis and catalytic application of ceria nanomaterials, Dalton Trans. 41 (2012) 14455-14475.

[3] A. Trovarelli, J. Llorca, Ceria catalysts at nanoscale: How do crystal shapes shape catalysis?, ACS Catal. 7 (2017) 4716-4735.

[4] M. Yang, D.S. Kim, J.-W. Sim, J.-M. Jeong, D.H. Kim, J.H. Choi, J. Kim, S.-S. Kim, B.G. Choi, Synthesis of vertical MnO_2 wire arrays on hemp-derived carbon for efficient and robust green catalysts, Appl. Surf. Sci. 407 (2017) 540-545.

[5] X. Huang, L. Liu, H. Gao, W. Dong, M. Yang, G. Wang, Hierarchically nanostructured $MnCo_2O_4$ as active catalysts for the synthesis of N-benzylideneaniline from benzyl alcohol and aniline, Green Chem. 19 (2017) 769-777.

[6] C. Perdomo, A. Pérez, R. Molina, S. Moreno, Storage capacity and oxygen mobility in mixed oxides from transition metals promoted by cerium, Appl. Surf. Sci. 383 (2016) 42-48.

[7] S. Liang, F. Teng, G. Bulgan, R. Zong, Y. Zhu, Effect of phase structure of MnO_2 nanorod catalyst on the activity for CO oxidation, J. Phys. Chem. C 112 (2008) 5307-5315.

[8] G. Zhao, J. Li, X. Ren, J. Hu, W. Hu, X. Wang, Highly active MnO_2 nanosheet synthesis from graphene oxide templates and their application in efficient oxidative degradation of methylene blue, RSC Adv. 3 (2013) 12909-12914.

[9] R. Xu, X. Wang, D.S. Wang, K.B. Zhou, Y.D. Li, Surface structure effects in nanocrystal MnO_2 and Ag/MnO_2 catalytic oxidation of CO, J. Catal. 237 (2006) 426-430.

[10] S. Xie, H. Dai, J. Deng, H. Yang, W. Han, H. Arandiyan, G. Guo, Preparation and high catalytic performance of Au/3DOM Mn_2O_3 for the oxidation of carbon monoxide and toluene, J. Hazard. Mater. 279 (2014) 392-401.

[11] S.H. Xie, Y.X. Liu, J.G. Deng, X.T. Zhao, J. Yang, K.F. Zhang, Z. Han, H. Arandiyan, H.X. Dai, Effect of transition metal doping on the catalytic performance of Au-Pd/3DOM Mn_2O_3 for the oxidation of methane and o-xylene, Appl. Catal. B-Environ. 206 (2017) 221-232.

[12] Y. Zheng, W. Wang, D. Jiang, L. Zhang, X. Li, Z. Wang, Insights into the solar light driven thermocatalytic oxidation of VOCs over tunnel structured manganese oxides, Phys. Chem. Chem. Phys. 18 (2016) 18180-18186.

[13] J. Jia, P. Zhang, L. Chen, The effect of morphology of α-MnO_2 on catalytic decomposition of gaseous ozone, Catal. Sci. Technol. 6 (2016) 5841-5847.

[14] D. Li, W. Li, Y. Deng, X. Wu, N. Han, Y. Chen, Effective Ti doping of δ-MnO_2 via anion route for highly active catalytic combustion of benzene, J. Phys. Chem. C 120 (2016) 10275-10282.

[15] T. Uematsu, Y. Miyamoto, Y. Ogasawara, K. Suzuki, K. Yamaguchi, N. Mizuno, Molybdenum-doped α-MnO_2 as an efficient reusable heterogeneous catalyst for aerobic sulfide oxygenation, Catal. Sci. Technol. 6 (2016) 222-233.

[16] Y.-X. Miao, L.-H. Ren, L. Shi, W.-C. Li, Hydrothermal synthesis of manganese oxide nanorods as a highly active support for gold nanoparticles in CO oxidation and their stability

at low temperature, RSC Adv. 5 (2015) 62732-62738.

[17] R. Xu, X. Wang, D. Wang, K. Zhou, Y. Li, Surface structure effects in nanocrystal MnO_2 and Ag/MnO_2 catalytic oxidation of CO, J. Catal. 237 (2006) 426-430.

[18] S. Zhang, Q. Fan, H. Gao, Y. Huang, X. Liu, J. Li, X. Xu, X. Wang, Formation of $Fe_3O_4@MnO_2$ ball-in-ball hollow spheres as a high performance catalyst with enhanced catalytic performances, J. Mater. Chem. A 4 (2016) 1414-1422.

[19] A. Trovarelli, Catalytic properties of ceria and CeO_2-containing materials, Catal. Rev. 38 (1996) 439-520.

[20] S. Carrettin, P. Concepcion, A. Corma, J.M.L. Nieto, V.F. Puntes, Nanocrystalline CeO_2 increases the activity of an for CO oxidation by two orders of magnitude, Angew. Chem. Int. Ed. 43 (2004) 2538-2540.

[21] J. Guzman, S. Carrettin, A. Corma, Spectroscopic evidence for the supply of reactive Oxygen during CO oxidation catalyzed by gold supported on nanocrystalline CeO_2, J. Am. Chem. Soc. 127 (2005) 3286-3287.

[22] S.H. Xie, Y.X. Liu, J.G. Deng, X.T. Zhao, J. Yang, K.F. Zhang, Z. Han, H.X. Dai, Three-dimensionally ordered macroporous CeO_2-supported Pd@Co nanoparticles: Highly active catalysts for methane oxidation, J. Catal., 342 (2016) 17-26.

[23] D. Tian, C. Zeng, H. Wang, X. Cheng, Y. Zheng, C. Xiang, Y. Wei, K. Li, X. Zhu, Effect of transition metal Fe adsorption on CeO2 (110) surface in the methane activation and oxygen vacancy formation: A density functional theory study, Appl. Surf. Sci. 416 (2017) 547-564.

[24] X. Huang, C. Ni, G. Zhao, J.T.S. Irvine, Oxygen storage capacity and thermal stability of the $CuMnO_2$-CeO_2 composite system, J. Mater. Chem. A 3 (2015) 12958-12964.

[25] D. Zhang, L. Zhang, L. Shi, C. Fang, H. Li, R. Gao, L. Huang, J. Zhang, In situ supported MnO_x-CeO_x on carbon nanotubes for the low-temperature selective catalytic reduction of NO with NH_3, Nanoscale 5 (2013) 1127-1136.

[26] Q. Shen, L. Zhang, N. Sun, H. Wang, L. Zhong, C. He, W. Wei, Y. Sun, Hollow MnO_x-CeO_2 mixed oxides as highly efficient catalysts in NO oxidation, Chem. Eng. J. 322 (2017) 46-55.

[27] P. Zhang, H. Lu, Y. Zhou, L. Zhang, Z. Wu, S. Yang, H. Shi, Q. Zhu, Y. Chen, S. Dai, Mesoporous $MnCeO_x$ solid solutions for low temperature and selective oxidation of hydrocarbons, Nat. Commun. 6 (2015) 8446.

[28] X. Han, C. Li, X. Liu, Q. Xia, Y. Wang, Selective oxidation of 5-hydroxymethylfurfural to 2,5-furandicarboxylic acid over MnO_x-CeO_2 composite catalysts, Green Chem. 19 (2017) 996-1004.

[29] D. Jampaiah, K.M. Tur, P. Venkataswamy, S.J. Ippolito, Y.M. Sabri, J. Tardio, S.K. Bhargava, B.M. Reddy, Catalytic oxidation and adsorption of elemental mercury over nanostructured CeO_2-MnO_x catalyst, RSC Adv. 5 (2015) 30331-30341.

[30] D. Jampaiah, P. Venkataswamy, K.M. Tur, S.J. Ippolito, S.K. Bhargava, B.M. Reddy, Effect of MnO_x loading on structural, surface, and catalytic properties of CeO_2-MnO_x mixed oxides prepared by sol-gel method, Z. Anorg. Allg. Chem. 641 (2015) 1141-1149.

[31] X. Wang, Y. Li, Synthesis and formation mechanism of manganese dioxide nanowires/canorods, Chem. Eur. J. 9 (2003) 300-306.

[32] C. Pan, D. Zhang, L. Shi, J. Fang, Template-free synthesis, controlled conversion, and CO oxidation properties of CeO_2 nanorods, nanotubes, nanowires, and nanocubes, Eur. J. Inorg. Chem. 2008 (2008) 2429-2436.

[33] X. Wang, Y.D. Li, Synthesis and formation mechanism of manganese dioxide nanowires/nanorods, Chemistry-a European Journal, 9 (2003) 300-306.

[34] X. Tang, J. Li, L. Sun, J. Hao, Origination of N_2O from NO reduction by NH_3 over β-MnO_2 and α-Mn_2O_3, Appl. Catal. B-Environ. 99 (2010) 156-162.

[35] V. Subramanian, H. Zhu, R. Vajtai, P.M. Ajayan, B. Wei, Hydrothermal synthesis and pseudocapacitance properties of MnO_2 nanostructures, J. Phys. Chem. B 109 (2005) 20207-20214.

[36] M.C. Biesinger, B.P. Payne, A.P. Grosvenor, L.W.M. Lau, A.R. Gerson, R.S.C. Smart, Resolving surface chemical states in XPS analysis of first row transition metals, oxides and hydroxides: Cr, Mn, Fe, Co and Ni, Appl. Surf. Sci. 257 (2011) 2717-2730.

[37] D. Jampaiah, V.K. Velisoju, P. Venkataswamy, V.E. Coyle, A. Nafady, B.M. Reddy, S.K. Bhargava, Nanowire morphology of mono- and bidoped α-MnO_2 catalysts for remarkable enhancement in soot oxidation, ACS Appl. Mater. Interfaces 9 (2017) 32652-32666.

[38] M.V. Rama Rao, T. Shripathi, Photoelectron spectroscopic study of X-ray induced reduction of CeO_2, J. Electron Spectrosc. Relat. Phenom. 87 (1997) 121-126.

[39] D. Jiang, W. Wang, E. Gao, S. Sun, L. Zhang, Highly selective defect-mediated photochemical CO_2 conversion over fluorite ceria under ambient conditions, Chem. Commun. 50 (2014) 2005-2007.

[40] G. Avgouropoulos, T. Ioannides, Effect of synthesis parameters on catalytic properties of CuO-CeO_2, Appl. Catal. B-Environ. 67 (2006) 1-11.

[41] B.M. Reddy, K.N. Rao, P. Bharali, Copper promoted cobalt and nickel catalysts supported on ceria−alumina mixed oxide: Structural characterization and CO oxidation activity, Ind. Eng. Chem. Res. 48 (2009) 8478-8486.

[42] J. Zhang, H. Kumagai, K. Yamamura, S. Ohara, S. Takami, A. Morikawa, H. Shinjoh, K. Kaneko, T. Adschiri, A. Suda, Extra-low-temperature oxygen storage capacity of CeO_2 nanocrystals with cubic facets, Nano Lett. 11 (2011) 361-364.

[43] H.J. Li, G.S. Qi, Tana, X.J. Zhang, X.M. Huang, W. Li, W.J. Shen, Low-temperature oxidation of ethanol over a $Mn_{0.6}Ce_{0.4}O_2$ mixed oxide, Appl. Catal. B-Environ. 103 (2011) 54-61.

[44] X. Tang, Y. Li, X. Huang, Y. Xu, H. Zhu, J. Wang, W. Shen, MnO_x–CeO_2 mixed oxide catalysts for complete oxidation of formaldehyde: Effect of preparation method and calcination temperature, Appl. Catal. B-Environ. 62 (2006) 265-273.

[45] Z. Yuan, S. Chen, B. Liu, Nitrogen-doped reduced graphene oxide-supported Mn_3O_4: An efficient heterogeneous catalyst for the oxidation of vanillyl alcohol to vanillin, J. Mater. Sci. 52 (2017) 164-172.

[46] M.T. Qamar, M. Aslam, Z.A. Rehan, M.T. Soomro, J.M. Basahi, I.M.I. Ismail, T. Almeelbi, A. Hameed, The influence of p-type Mn_3O_4 nanostructures on the photocatalytic activity of ZnO for the removal of bromo and chlorophenol in natural sunlight exposure, Appl. Catal. B-Environ. 201 (2017) 105-118.

[47] E.S. Ilton, J.E. Post, P.J. Heaney, F.T. Ling, S.N. Kerisit, XPS determination of Mn oxidation states in Mn (hydr)oxides, Appl. Surf. Sci. 366 (2016) 475-485.

[48] Y. Yang, Z.-C. Zhang, P.-P. Wang, J.-C. Zhang, F. Nosheen, J. Zhuang, X. Wang, Hierarchical MnO_2/SnO_2 Heterostructures for a novel free-standing ternary thermite membrane, Inorg. Chem. 52 (2013) 9449-9455.

[49] G. Du, X. Liu, Y. Zong, T.S.A. Hor, A. Yu, Z. Liu, Co_3O_4 nanoparticle-modified MnO_2 nanotube bifunctional oxygen cathode catalysts for rechargeable zinc-air batteries, Nanoscale 5 (2013) 4657-4661.

[50] H.-X. Mai, L.-D. Sun, Y.-W. Zhang, R. Si, W. Feng, H.-P. Zhang, H.-C. Liu, C.-H. Yan, Shape-selective synthesis and oxygen storage behavior of ceria nanopolyhedra, nanorods, and nanocubes, J. Phys. Chem. B 109 (2005) 24380-24385.

[51] X. Liu, K. Zhou, L. Wang, B. Wang, Y. Li, Oxygen vacancy clusters promoting reducibility and activity of ceria nanorods, J. Am. Chem. Soc. 131 (2009) 3140-3141.

[52] Y. Wei, J. Liu, W. Su, Y. Sun, Y. Zhao, Controllable synthesis of Ce-doped α-MnO_2 for low-temperature selective catalytic reduction of NO, Catal. Sci. Technol. 7 (2017) 1565-1572.

Figure Captions

Fig. 1. XRD patterns: (a) β-MnO_2, (b) $CeO_{2-\delta}$@β-MnO_2, (c) $CeO_{2-\delta}$-β-MnO_2, and (d) $CeO_{2-\delta}$.

Fig. 2. FESEM (a, c, e, g) and TEM (b, d, f, h) images: (a, b) $CeO_{2-\delta}$, (c, d) β-MnO_2, (e, f) $CeO_{2-\delta}$@β-MnO_2, and (g, h) $CeO_{2-\delta}$-β-MnO_2.

Fig. 3. XPS spectra of $CeO_{2-\delta}$@β-MnO_2: (a) Mn 2p, (b) Ce 3d, and (c) O 1s.

Fig. 4. H_2-TPR results for $CeO_{2-\delta}$, β-MnO_2, $CeO_{2-\delta}$@β-MnO_2 and $CeO_{2-\delta}$-β-MnO_2.

Fig. 5. TGA of synthesized samples under flowing (a) air, (b) pure N_2, and (c) 5%H_2/95%Ar.

Fig. 6. (a) Mn 2p and (b) Mn 3s XPS spectra of $CeO_{2-\delta}$@β-MnO_2 after TGA test from room temperature to 800 ^oC under flowing N_2.

Fig. 7. In-situ high-temperature XRD patterns using Mo K alpha as radiation for $CeO_{2-\delta}$@β-MnO_2 under N_2 with the increasing of temperature from room temperature to 800 ^oC with 100 ^oC step.

Fig. 8. XRD patterns for β-MnO_2: (a) fresh sample from hydrothermal reaction, (b) treated under flowing N_2 at 300 ^oC for 2 h.

Scheme 1: Proposed mechanism of $CeO_{2-\delta}$@β-MnO_2 formation and their enhanced oxygen transfer properties.

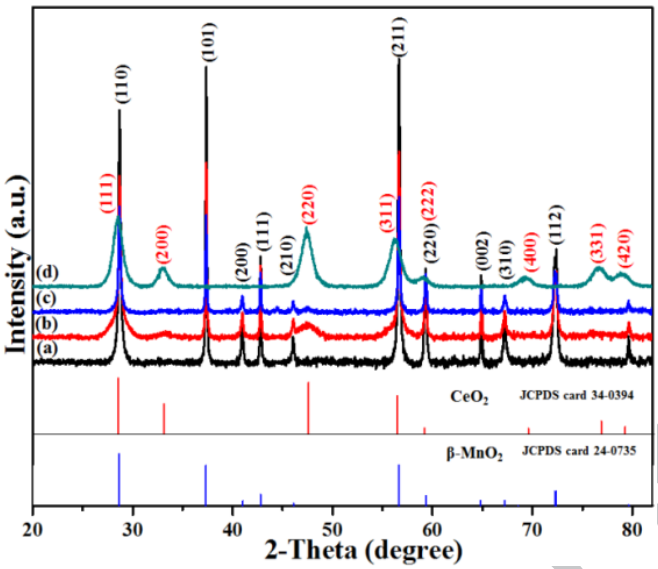

Fig. 1

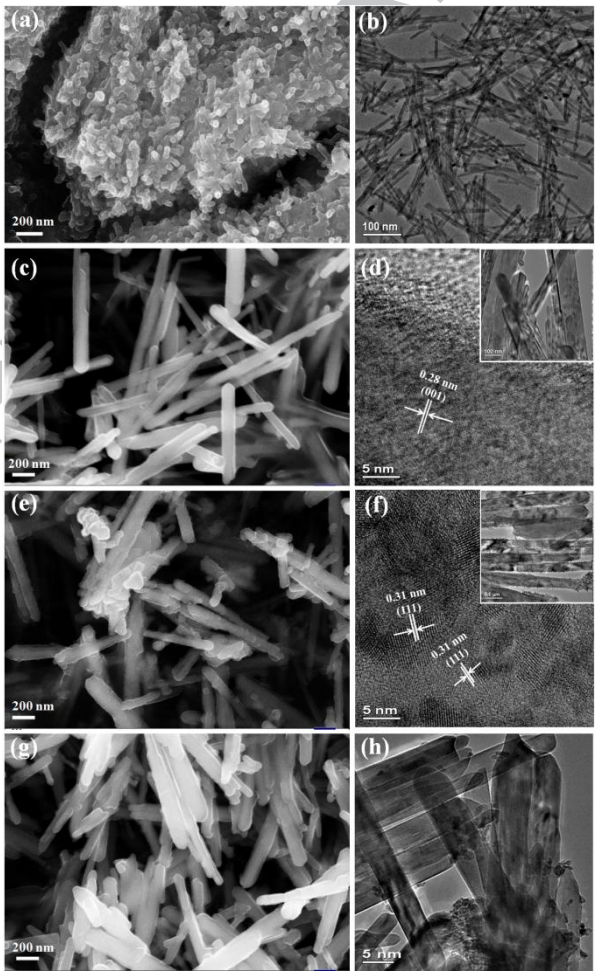

Fig. 2

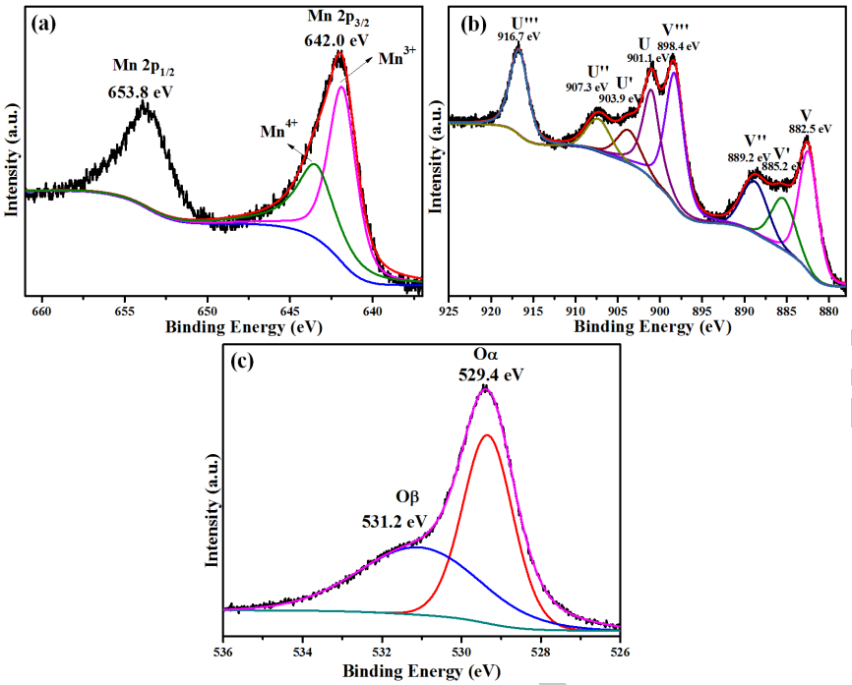

Fig. 3

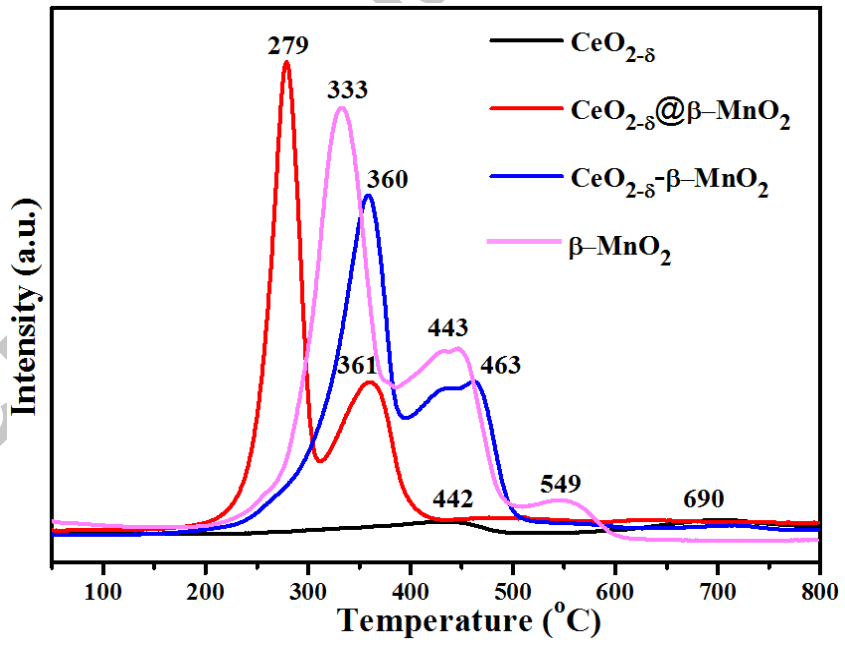

Fig. 4

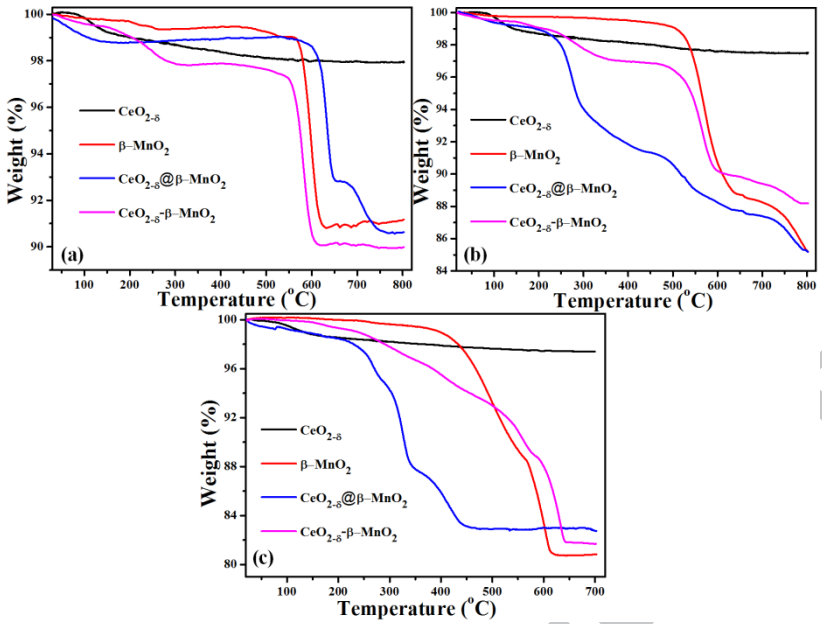

Fig. 5

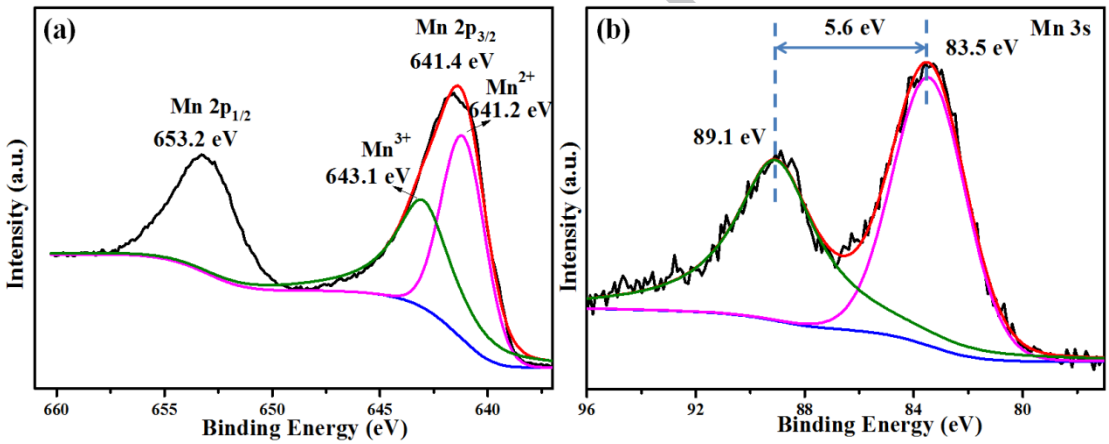

Fig. 6

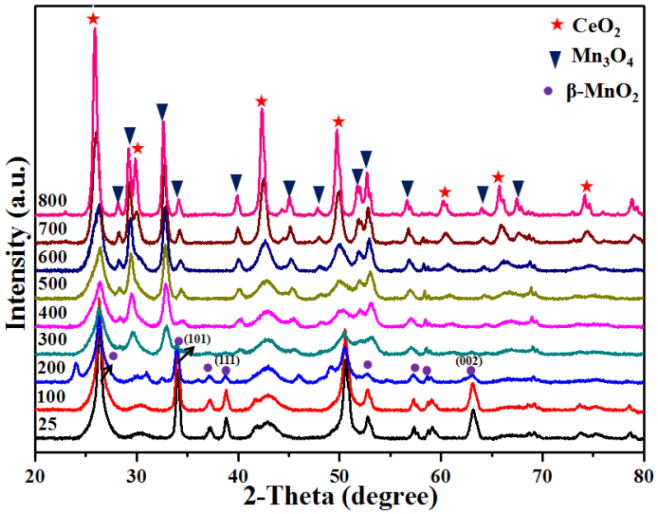

Fig. 7

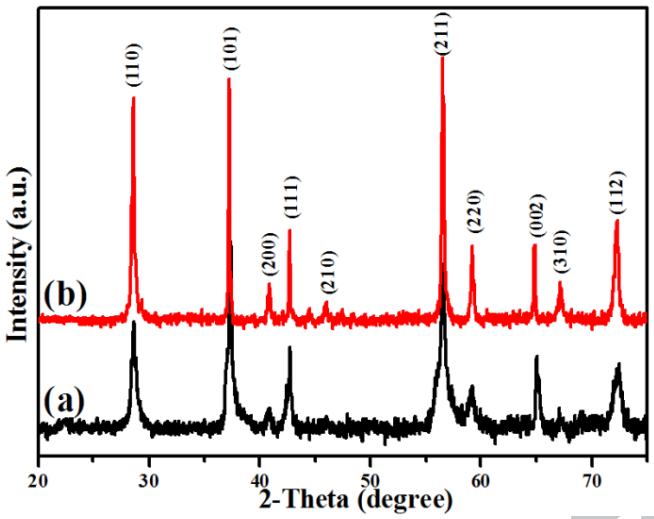

Fig. 8

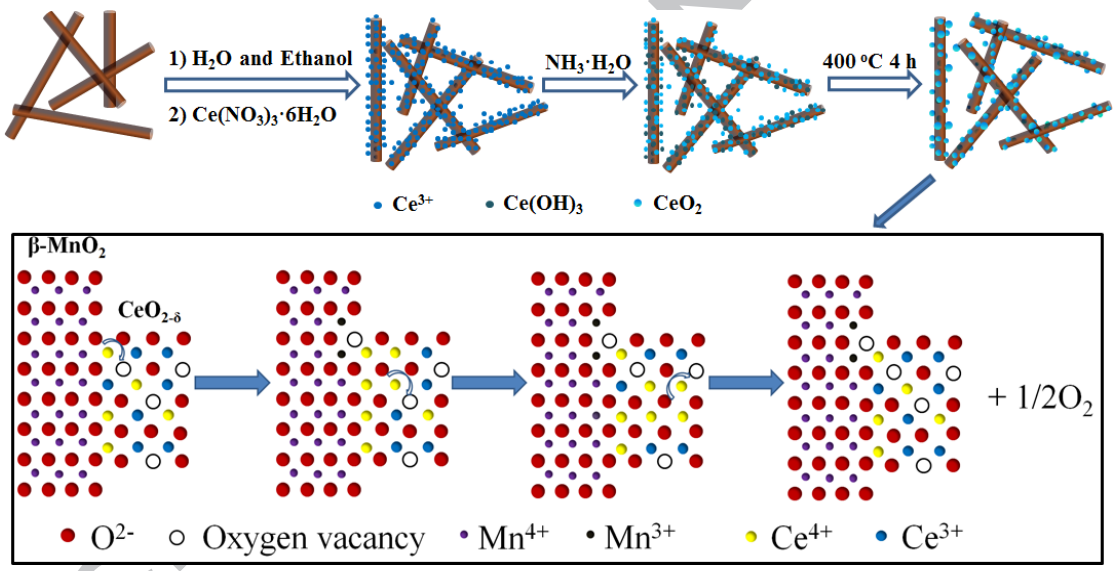

Scheme 1

Table 1 Weight loss steps and temperature ranges of samples under various kinds of flowing gases

Sample	Air		Pure N_2		5%H_2/95%Ar	
	Temperature (^oC)	Weight loss (wt%)	Temperature (^oC)	Weight loss (wt%)	Temperature (^oC)	Weight loss (wt%)
$CeO_{2-\delta}$	30-300	1.3	30-400	1.9	30-350	2.0
	300-650	0.7	400-650	0.6	350-550	0.5
	650-800	<0.1	650-800	<0.1	550-700	0.1
β-MnO_2	30-300	0.7	100-400	0.3	100-350	0.5
	550-650	8.3	400-650	11.0	300-550	10.3
	650-800	<0.1	650-800	3.3	550-700	8.5
$CeO_{2-\delta}$@β-MnO_2	30-300	1.2	100-400	**7.5**	100-350	**11.4**
	550-650	6.0	400-650	4.1	350-550	4.9
	650-800	2.2	650-800	2.5	550-700	0.2
$CeO_{2-\delta}$-β-MnO_2	30-300	2.1	100-400	2.5	100-350	3.3
	500-650	7.9	400-650	7.2	350-550	5.8
	650-800	<0.1	650-800	1.6	550-700	9.2

Graphical abstract

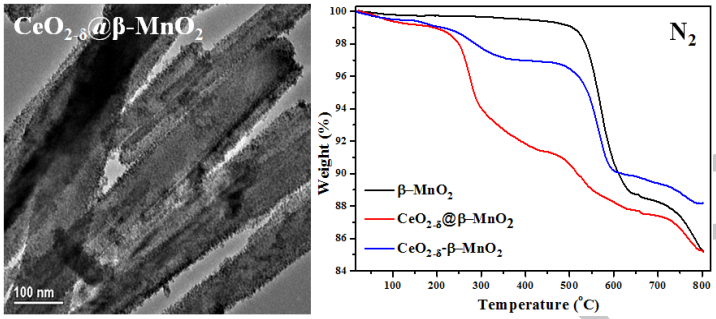

Highlights

- Nanocrystalline $CeO_{2-\delta}$ coated β-MnO_2 nanorods have been prepared.
- $CeO_{2-\delta}$ coating facilitates the oxygen transfer in β-MnO_2 nanorods under inert or reductive atmospheres.
- $CeO_{2-\delta}$ nanocrystals act as oxygen transfer channels between the well-interacted $CeO_{2-\delta}$ and β-MnO_2 nanorods.